

## 2. ALTERATION EFFECTS ON PETROPHYSICAL PROPERTIES OF SUBAERIAL FLOOD BASALTS: SITE 990, SOUTHEAST GREENLAND MARGIN<sup>1</sup>

Sverre Planke,<sup>2</sup> Brian Cerney,<sup>3</sup> Christian J. Bucker,<sup>4</sup> and Odd Nilsen<sup>2</sup>

### ABSTRACT

Ocean Drilling Program Hole 990A penetrated 131 m of subaerially emplaced Paleocene flood basalts on the Southeast Greenland margin with a recovery of 74%. Shipboard  $P$ -wave velocity ( $V_p$ ), density, and magnetic susceptibility were measured with 2- to 15-cm intervals on the core. Individual flow units were divided into four zones based on the observed petrophysical characteristics. From the top, these are Zone I (<7 m thick with a  $V_p$  of ~2.5 km/s), Zone II (3–5 m thick with a strongly increasing  $V_p$  from 2.5 to 5.5 km/s), Zone III (up to 20 m thick with a  $V_p$  of ~5.5–6.0 km/s), and Zone IV (<2 m thick with a strongly decreasing  $V_p$  from 6.0 to 2.5 km/s). Eighteen samples were selected from three of the fourteen penetrated basalt units for geochemical, petrological, and petrophysical studies focusing on the altered, low-velocity upper lava Zones I and II. Zone I is strongly altered to >50% clay minerals (smectite) and iron hydroxides, and the petrophysical properties are primarily determined by the clay properties. Zone II is intermediately altered with 5%–20% clay minerals, where the petrophysical properties are a function of both the degree of alteration and porosity variations. Shipboard and shore-based measurements of the same samples show that storage permanently lowers the elastic moduli of basalt from Zones I to III. This is related to the presence of even small quantities of swelling clays. The data show that alteration processes are important in determining the overall seismic properties of flood basalt constructions. The degree and depth of alteration is dependent on the primary lava flow emplacement structures and environment. Thus, the interplay of primary emplacement and secondary alteration structures determine the elastic properties of basalt piles. Rock property theories for sand-clay systems are further used to model the physical property variations in these altered crystalline rocks.

### INTRODUCTION

Wireline log data recorded in subaerial flood basalt constructions show a characteristic cyclic pattern, with large variations in elastic parameters within individual basalt units (Planke, 1994; Delius et al., 1995; Planke and Cambray, 1998). Typically, the  $P$ -wave velocity ( $V_p$ ) is as low as 2–3 km/s in the basalt top, but increases to 5.5–6 km/s in the interior of lavas thicker than 5–10 m and decreases rapidly near the lava base. This three-part flow zonation is very similar to observations of textural characteristics revealed by field studies of inflated flood basalt lavas, with an upper vesicular crust, a central massive and fractured core, and a thin basal vesicular crust (Self et al., 1997, 1998).

Continental breakup is frequently associated with voluminous volcanism. Seismic data are essential for mapping the aerial distribution of the volcanic constructions along rifted margins. Seismic imaging of intra- and sub-basalt features is generally difficult. The large variations in seismic properties in single subaerial lava flows give rise to numerous high-impedance boundaries within the flood basalt constructions. Because the dominant wavelength of 50–100 m used in conventional seismic experiments is much larger than the typical thickness of a flood basalt unit, a reflected wave field in these terrains will consist of strong reverberations and tuned waves (Planke and Eldholm, 1994). However, well-defined intra- and sub-basalt reflectivity is imaged on modern seismic reflection profiles (e.g., Symonds et al., 1998). Improved understanding of the seismic

properties of individual basalt flows may help to improve the seismic imaging capability in volcanic terrains.

During Leg 163, Hole 990A was drilled 131 m into basaltic basement, penetrating 14 subaerial flood basalt units with an excellent average recovery of 74% (Fig. 1) (Duncan, Larsen, Allan, et al., 1996). The recovery is biased toward sampling the massive flow interiors as shown by (1) a recovery of 30%–60% in many of the cores penetrating unit boundaries, compared with the 74% average recovery and (2) only 2 of 14 unit boundaries were recovered.  $P$ -wave velocity, gamma-ray attenuation porosity evaluator (GRAPE) density and magnetic susceptibility were measured shipboard at 2–15-cm core intervals (Fig. 2). Unfortunately, the hole was not logged because of bad weather. However, the high recovery and closely spaced shipboard measurements allow detailed studies of systematic intrabasalt physical property variations.

This paper focuses on how the interplay of primary emplacement structures (such as vesicularity and fractures) and subsequent alteration determine the large variations in physical properties observed in the top part of the basalt flows. We investigated in detail the changing textural, mineralogical, and physical property variations in the top part of three representative and well-sampled basalt flows. Cerney and Carlson (Chap. 3, this volume) describe the velocity variations in the massive part of the lavas from modeling of high-pressure  $P$ - and  $S$ -wave minicore velocity measurements. They show that the velocity distribution can be explained by variations in porosity and a common pore aspect ratio distribution.

### SITE 990

Eight sites were drilled along the EG63 transect on the Southeast Greenland margin during Legs 152 and 163 (Fig. 1) (Larsen and Saunders, 1998). At Hole 990A we penetrated 212 m of sediment and 131 m of basaltic basement at a water depth of 540 m (Duncan, Larsen, Allan, et al., 1996). The goal for this site was to drill deeper than in the

<sup>1</sup>Larsen, H.C., Duncan, R.A., Allan, J.F., Brooks, K. (Eds.), 1999. *Proc. ODP, Sci. Results*, 163: College Station, TX (Ocean Drilling Program).

<sup>2</sup>Department of Geology, University of Oslo, Box 1047 Blindern, 0316 Oslo, Norway, planke@geologi.uio.no

<sup>3</sup>Department of Geology and Geophysics, Texas A&M University, College Station, TX 77843-3114, U.S.A.

<sup>4</sup>Joint Geoscientific Institute of the State Geological Surveys, Stilleweg 2, D-30655 Hannover, Federal Republic of Germany.

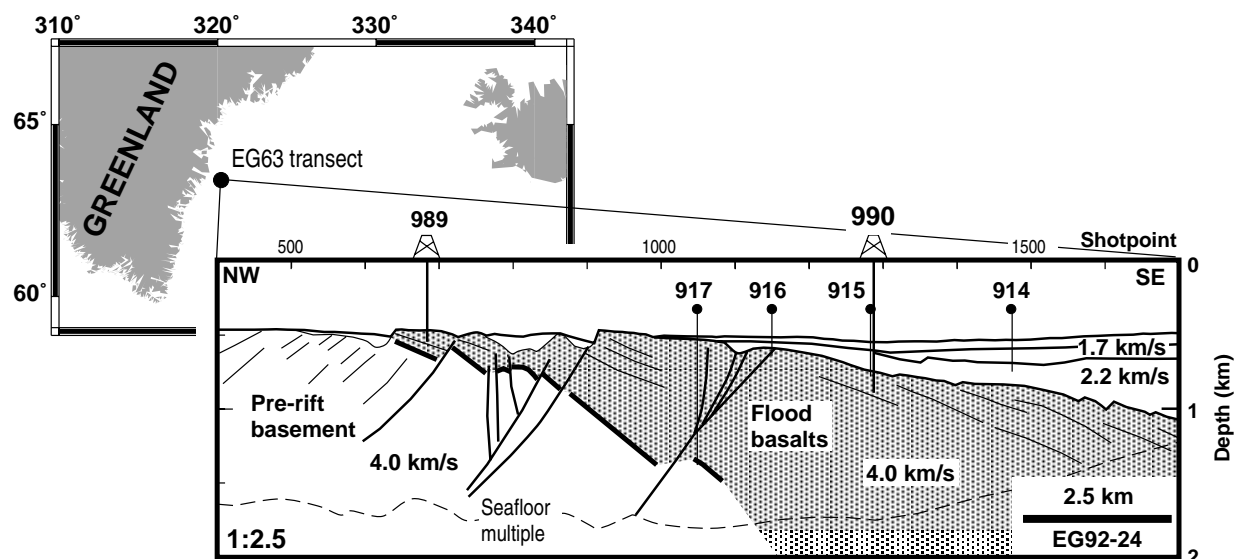


Figure 1. Depth-converted interpretative line drawing of the inner part of the EG63 transect showing Legs 152 and 163 drill sites. Based on Duncan, Larsen, Allan, et al. (1996).

nearby Site 915 to obtain a complete volcanostratigraphic section at the inner part of the EG63 transect. Fourteen subaerially emplaced basaltic flow units were identified, consisting of a mixture of dominantly plagioclase-olivine phyric basalt and aphyric basalt (Fig. 2). The units are classified as aa (four upper units), transitional (four middle units) and pahoehoe (five lower units). A downhole decrease in unit thickness was observed.

The core recovery in the massive interior of the lavas was often complete. A number of cores actually had a recovery of >100%, being related to inaccuracies in the driller's depth, spaces in the curated core, and possible recovery of core drilled during the previous drilling. In contrast, recovery in the top and base of the flow units is lower, frequently 30%–60%.

Units 2 and 9 and Subunit 3A were chosen for detailed studies of petrophysical properties near the flow boundaries. Unit 2 and Subunit 3A are thick aa basalts with well-defined weathered flow tops; Unit 9 is a very vesicular pahoehoe basalt (Fig. 2; Table 1). The massive interior of the units was almost completely recovered. Based on the general high recovery of the massive part of the units, we interpret the missing section in Cores 8R and 12R (Fig. 2) to belong to the strongly altered flow top. Eighteen minicore samples were selected from these three units for further studies.

## DATA ANALYSIS

### Shipboard Measurements

Bulk GRAPE density and magnetic susceptibility were measured on whole-round cores at a 2-cm sampling interval on the multisensor track (MST) immediately after the core was brought on deck (Duncan, Larsen, Allan, et al., 1996).  $P$ -wave velocities were then measured on split cores at 5–15-cm intervals in the Hamilton Frame velocimeter as soon as possible after the core was split to ensure water saturation and minimum relaxation cracking. In addition,  $V_p$ , density, and porosity were measured later in 51 minicores using standard shipboard procedures described by Larsen, Saunders, Clift, et al. (1994).

### Physical Properties

$P$ - and  $S$ -wave velocity, density, and porosity were measured on 14 of the samples by the Norwegian Geotechnical Institute (NGI) (Table 2). Dry and saturated weights were initially measured. Average bulk volume was determined from water-saturated samples by (1) averaging volume estimates from vernier measurements of the average of three diameters and three lengths and (2) measuring the immersed weight of the cores. Bulk and dry densities were calculated from the saturated and dry weights, respectively, divided by the average volume. The porosity was obtained from the difference in bulk and dry density. Velocities were measured on water-saturated cores using contact transducers under atmospheric conditions. A 500-kHz  $P$ -wave transducer and a 250-kHz  $S$ -wave transducer were used, and transit times were picked manually. Velocities were also measured under 10–200-MPa confining pressure on 13 other minicores collected from the massive basalt interior (Cerney and Carlson, Chap. 3, this volume). The altered samples analyzed in this study were regarded as too fragile to obtain reliable high-pressure velocity measurements. Finally, magnetic properties were measured by Norges Geologiske Undersøkelser (NGU) on ten minicores. Magnetic remanence was measured using a JR5 magnetometer; volume susceptibility, using a Bartington MS2; and Curie temperature, using a horizontal translation balance.

### Petrology and Geochemistry

Unpolished thin sections and powder were made from the 18 samples. Eight thin sections from massive minicores were subsequently polished for identification of magnetic minerals. Major element X-ray fluorescence (XRF) and bulk normal and clay-sized (<2  $\mu\text{m}$  fraction) X-ray diffraction (XRD) analyses were carried out at the University of Oslo using standard procedures. XRD runs on the clay-sized fractions were done on bulk, heat-treated (550°C), and ethylene glycol-treated filtrate. Mineral identification and modal analysis of the diffractograms (Table 2) were done using the MacDiff software (Petschink, 1997).

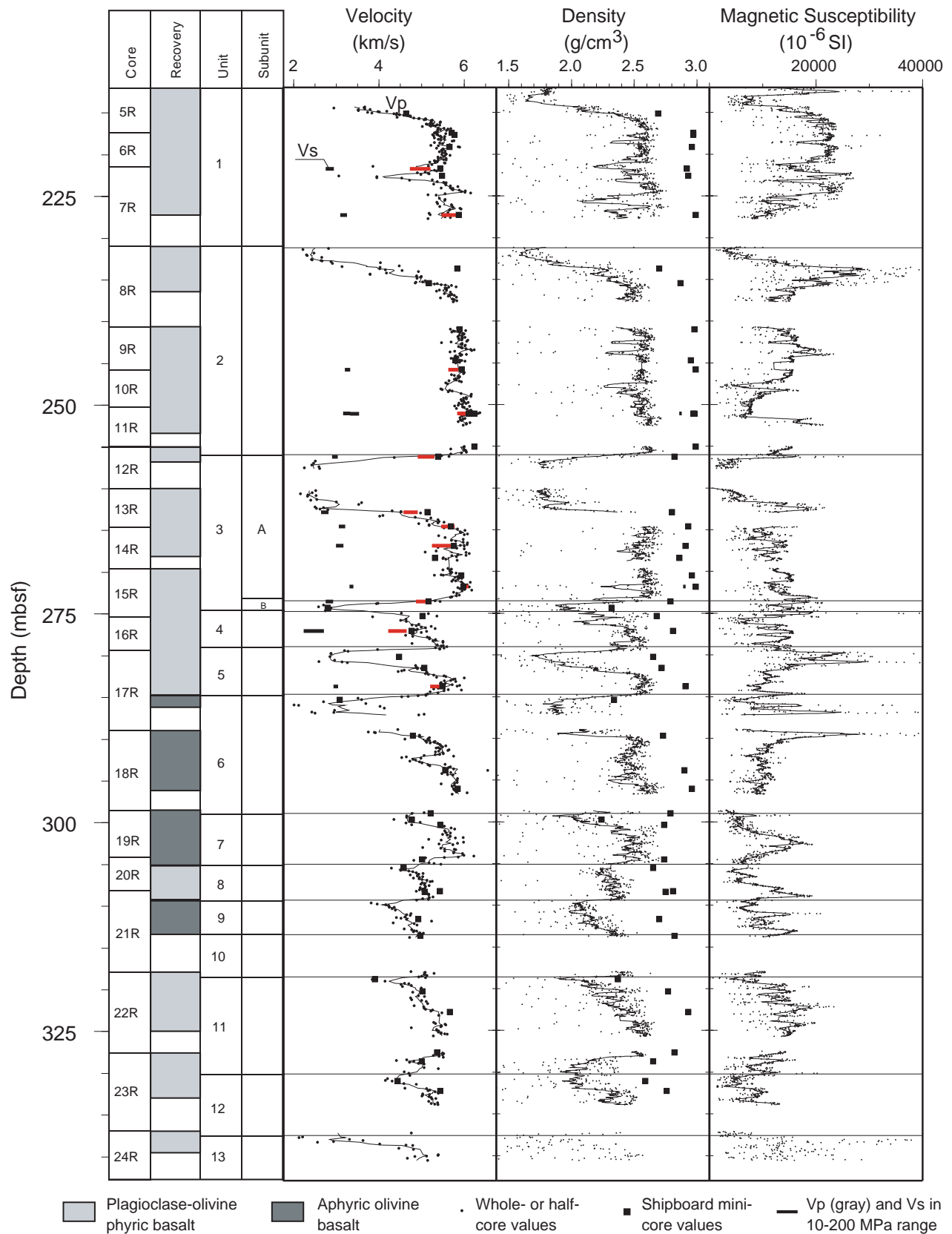


Figure 2. Summary of Hole 990A volcanostratigraphy and physical property measurements. Solid lines = running-average filtered data. Filter length = 5 samples (velocity) and 15 samples (density and magnetic susceptibility). Curator depth scale used; measurements on adjacent cores with overlapping depth values removed. High-pressure velocity data from Cerney and Carlson (Chap. 3, this volume), other data from Shipboard Scientific Party (1996).

**Table 1. Summary of petrological and structural characteristics of three lava flows in Hole 990A.**

	Unit 2 Plagioclase-olivine phyric basalt	Unit 3A Plagioclase-olivine phyric basalt	Unit 9 Aphyric olivine basalt
Thickness (m)	24.8	17.5	4.1
Recovery (%)	89	83	110
Flow type	Aa	Aa	Pahoehoe
Boundary			
Upper	Not found. 8R-1 (15 cm).	5 mm red soil. 12R-2 (18 cm).	Not found. 21R-1 (127 cm).
Lower	5 mm red soil. 12R-2 (15 cm).	Not found. 15R-4 (20 cm).	Not found. 21R-4 (145 cm).
Internal Structure			
Top breccia	Recovery = 1.9 m, max.* = 6.1 m. Dark reddish brown to dusky red.	Recovery = 3.7 m, max.* = 7.0 m. Dark reddish brown to dusky red.	None.
Interior	Massive. Subhorizontal flow-banding common. Medium gray; reddening towards base.	Massive. Flow-banding or mesostasis-rich wisps common. Medium gray; dusky red to pinkish red in top meter.	Massive. Pinkish gray changing to greenish gray downwards.
Basal breccia	Recovery = 0.2 m, max.* = 3.5 m. Dark reddish brown.	Recovery = 0.2 m, max.* = 0.5 m. Dark reddish gray.	None.
Vesicles	<i>Breccia</i> : 0%–5%, open in top; 10%–15% open and clay-filled in base. <i>Interior</i> : 1%, filled with clay; a few small highly vesicular patches. Up to 12% in lower 30 cm.	<i>Breccia</i> : 1%–20%, open and zeolite or clay-filled in top; 10%, open, in base. <i>Interior</i> : 1%, filled; open, high-vesicularity bands in upper 7 m. Increasing from 1% to 10% in lower 3 m.	Very vesicular. 15%–25% in upper 3 m; lower meter fairly dense. Dominantly open; downward increase in size.
Veins/fractures	None to <1%, up to 4 mm wide, random to steeply inclined, filled with clay, zeolites and calcite. 5% subvertical fractures with slickensides in 1-m interval 10 m above base.	None to <1%, up to 2 mm wide, mainly steeply inclined, filled with clay, zeolites and calcite.	One 0.1 mm subvertical vein.
Mineralogy & Alteration			
Phenocrysts	<i>Plagioclase</i> : 5%–15%, up to 5 mm, decreasing size and number in lower part. <i>Olivine</i> : <1%, up to 1-2 mm, replaced by green clay.	<i>Plagioclase</i> : 5%–10%, up to 3 mm. <i>Olivine</i> : 5%, up to 1 mm. <i>Clinopyroxene</i> : Traces, 0.5 mm, in lower part.	Aphyric. Traces of olivine.
Groundmass	Fine-grained; top-part microcrystalline.	Fine-grained; top-part microcrystalline.	Fine-grained.
Alteration	<i>Breccia</i> : high. <i>Interior</i> : moderate; high just above base.	<i>Breccia</i> : high. <i>Interior</i> : moderate, high just below top and above base. Olivine phenocrysts replaced by clay.	High; moderate in lower meter.

Notes: \* = The maximum thickness is the sum of recovered and not recovered section in cores with breccia. Data from Duncan, Larsen, Allan, et al. (1996).

## RESULTS—UNITS 2 AND 9 AND SUBUNIT 3A

### Petrology and Geochemistry

The textural and mineralogical characteristics of the samples show that they can be divided into three major groups (Figs. 3, 4; Table 2). Group 1 samples are almost completely altered basalt from the brecciated flow top, while Group 3 samples are massive basalts from the interior of the lavas with little alteration. Group 2 samples are altered basalt in the transition zone between the massive interior and brecciated flow top, but also include altered, highly vesicular samples.

#### Thin-section and X-Ray Diffraction Descriptions

Group 1 thin sections show highly vesicular lava broken into sub-angular fragments of partly devitrified glass. Pseudomorphs of non-aligned tablets of plagioclase were found in the vitreous groundmass with abundant dusty hematite and/or limonite. A few 0.1-mm olivine pseudomorphs were observed. Linings of chalcedony are abundant around the subangular scoria fragments and also where occasional phenocrysts of less altered clinopyroxene and impregnations of fine-grained magnetite are found. The modal XRD analysis shows 60%–80% clay and 20%–40% iron oxide.

Group 2 thin sections consist of subhedral and anhedral pseudomorphs of plagioclase and minor clinopyroxene and olivine phenocrysts. The 0.5- to 2-mm plagioclase phenocrysts are partially altered into microcrystalline clayey aggregates. The 0.2- to 0.5-mm olivine phenocrysts are completely altered into serpentine-chlorite-iddingsite aggregates, whereas the pyroxene phenocrysts appear virtually unaltered. The groundmass is a fine-grained plagioclase-magnetite-clinopyroxene matrix. Sparsely distributed vesicles lined with chalcedony are also characteristic. The modal XRD analysis shows about

30% plagioclase, 40%–50% pyroxene, 5%–15% clay, and 10%–20% iron oxides.

Group 3 thin sections consist of subhedral phenocrysts of plagioclase with grain sizes of 0.3–3.5 mm in an equigranular, fine-grained groundmass with grain sizes of 0.05–1 mm. The groundmass is composed of mainly clinopyroxene and plagioclase in an interlocking, nonaligned texture. Main accessory minerals are opaque ore minerals, chiefly magnetite, and olivine or olivine pseudomorphs as microcrystalline serpentine-chlorite-iddingsite aggregates. The modal XRD analysis shows 40%–50% plagioclase, 30%–40% pyroxene, ~5% olivine, and, finally, 10%–20% iron oxide.

The <2- $\mu$ m-fraction XRD diffractograms show that smectite is the dominant clay mineral in all samples. Traces of kaolinite are identified in four samples, whereas chlorite is identified as ~25% of the clay minerals in one sample.

#### X-Ray Fluorescence Analysis

The major element compositions (Table 2) show systematic variations in the lava units. There is a downward decrease in aluminum, iron, potassium, and titanium oxide content. In contrast, the calcium, sodium, and phosphor oxide content is increasing downwards. The systematic changes in major element composition generally correlate with the degree of alteration. A notable exception is the potassium oxide content—in Unit 2 and Subunit 3A, this is lower in the highly altered upper brecciated interval, containing >60% clay, than in the intermediately altered sections below, containing <10% clay.

### Physical Properties

#### Velocity

Shipboard measurements of seismic  $V_p$  in Unit 2 and Subunit 3A varies from 2.5 km/s in the brecciated flow top to 6 km/s in the mas-

**Table 2. Petrophysical, petrological, and geochemical data, Hole 990A.**

Core, section:	8R-1	8R-2	8R-3	8R-5	9R-2	10R-1	11R-1	12R-2	13R-1	13R-2	13R-2	13R-3	13R-3	14R-1	21R-2	21R-3	21R-4	21R-4
Interval (cm):	96-98	130-132	126-128	3-5	5-7	62-64	10-12	75-77	44-46	48-50	125-127	31-33	62-64	49-51	30-32	120-122	22-24	57-59
Unit:	2	2	2	2	2	2	2	3A	3A	3A	3A	3A	3A	3A	9	9	9	9
Depth (mbsf):	232.1	233.8	235.3	236.4	242.2	246.3	250.4	257.2	260.4	262.0	262.7	263.3	263.6	265.1	309.9	312.3	312.8	313.2
Depth from unit top (m):	0.9	2.6	4.1	5.2	11.0	15.1	19.2	1.2	4.4	6.0	6.7	7.3	7.6	9.1	0.5	2.9	3.4	3.8
$V_p$ (km/s)		3.53	4.37	4.69	5.11	5.07	5.11				3.69	3.62	4.40	5.00	3.24	4.23	4.04	4.09
$V_p$ smooth (km/s)	2.40	4.00	5.00	5.60	5.90	5.90	6.10	2.50	2.40	2.50	4.40	4.60	5.00	5.80	4.10	4.80	4.70	4.80
$V_p$ nearest (km/s)	2.30	4.15	5.02	5.35	5.88	5.98	6.10	2.42	2.45	3.53	4.30	4.09	5.22	6.02	4.16	4.89	4.59	4.81
$V_s$ (km/s)		2.16	2.64	2.24	2.90	2.34	2.90				2.13	2.17	2.47	2.74	2.04	2.43	2.30	2.51
Bulk density (g/cm <sup>3</sup> )		2.57	2.71	2.83	2.91	2.87	2.90				2.54	2.51	2.83	2.88	2.33	2.42	2.54	2.66
Dry Density (g/cm <sup>3</sup> )		2.52	2.49	2.79	2.89	2.85	2.89				2.44	2.43	2.80	2.86	2.22	2.35	2.51	2.60
Porosity (%)		5.43		3.60	1.57	2.43	1.56				9.96	8.29	3.51	1.48	10.47	7.42	2.80	6.11
Susceptibility (10 <sup>-6</sup> SI)			27721		16707	16158	17427	7045			22346	15480	32654	11127	8674			
Remanence (mA/M)			597		111	314	1572	64			3557	5523	338	797	5187			
Q-factor (F = 50,000 nT)			0.55		0.17	0.49	2.30	0.23			4.05	9.09	0.26	1.82	15.23			
Titanomagnetite			X	X	X	X	X					X	X					
Magnetite							X					X	X					X
Hematite			X	X	X								X	X				
Other magnetic minerals					Rutile	Martite	Ilmenite											
Geochemical group	1	2	2	3	3	3	3	1	1	1	2	2	3	3	2	3	3	3
Clinopyroxene (%)	Tr	48	42	41	35	38	39	Tr	Tr	Tr	51	39	38	35	42	38	38	36
Olivine (%)	Tr	Tr	3	Tr	6	Tr	4	Tr	Tr	Tr	Tr	Tr	6	5	Tr	6	Tr	Tr
Clay (%)	78	7	6	Tr	Tr	Tr	Tr	72	68	62	61	6	Tr	Tr	13	Tr	Tr	Tr
Iron oxide (%)	22	11	10	7	18	13	12	28	32	38	11	18	13	20	17	13	6	16
SiO <sub>2</sub>	49.97	49.08	48.98	49.43	49.75	49.49	48.53	49.54	48.91	48.79	48.63	48.94	48.19	49.74	50.70	49.49	49.72	50.05
Al <sub>2</sub> O <sub>3</sub>	17.15	15.01	15.11	15.51	15.40	15.46	14.72	17.33	16.01	15.87	15.84	15.32	14.33	14.86	13.50	13.12	15.36	15.26
Fe <sub>2</sub> O <sub>3</sub>	13.87	12.88	13.03	11.49	12.07	11.86	12.10	13.93	14.63	14.41	12.89	13.20	12.67	12.71	12.45	12.91	10.12	10.24
MnO	0.16	0.21	0.20	0.18	0.19	0.17	0.21	0.19	0.19	0.19	0.20	0.21	0.23	0.20	0.19	0.23	0.22	0.22
MgO	4.92	6.67	6.77	6.35	6.71	6.84	6.39	5.48	6.30	6.82	6.55	7.27	6.87	7.43	7.29	8.69	7.92	7.99
CaO	2.42	9.55	10.84	12.04	11.88	11.85	11.70	3.70	4.87	5.61	10.75	8.72	11.33	11.50	10.41	10.78	11.69	11.73
Na <sub>2</sub> O	1.92	2.02	2.13	2.23	2.22	2.29	2.00	1.64	1.59	1.40	1.98	1.59	1.89	2.08	2.00	1.82	2.25	2.15
K <sub>2</sub> O	0.34	0.50	0.37	0.21	0.22	0.17	0.15	0.21	0.24	0.26	0.38	0.27	0.21	0.18	0.24	0.16	0.11	0.09
TiO <sub>2</sub>	1.06	1.00	1.04	0.99	0.94	0.94	0.96	1.04	1.09	1.04	0.97	0.94	0.85	0.91	0.90	0.89	0.94	0.88
P <sub>2</sub> O <sub>5</sub>	0.04	0.08	0.09	0.11	0.09	0.08	0.08	0.03	0.06	0.02	0.07	0.06	0.06	0.07	0.09	0.07	0.08	0.08
LOI	6.41	2.23	0.77	0.36	0.04	0.08	0.01	6.40	5.61	5.25	1.61	3.29	0.55	0.59	1.60	1.64	0.56	0.99
SUM	98.26	99.23	99.33	98.90	99.51	99.23	96.85	99.49	99.50	99.66	99.87	99.81	97.18	100.27	99.37	99.80	98.97	99.68

Notes: The maximum thickness is the sum of recovered and not recovered section in cores with breccia. LOI = loss on ignition. Tr = trace.

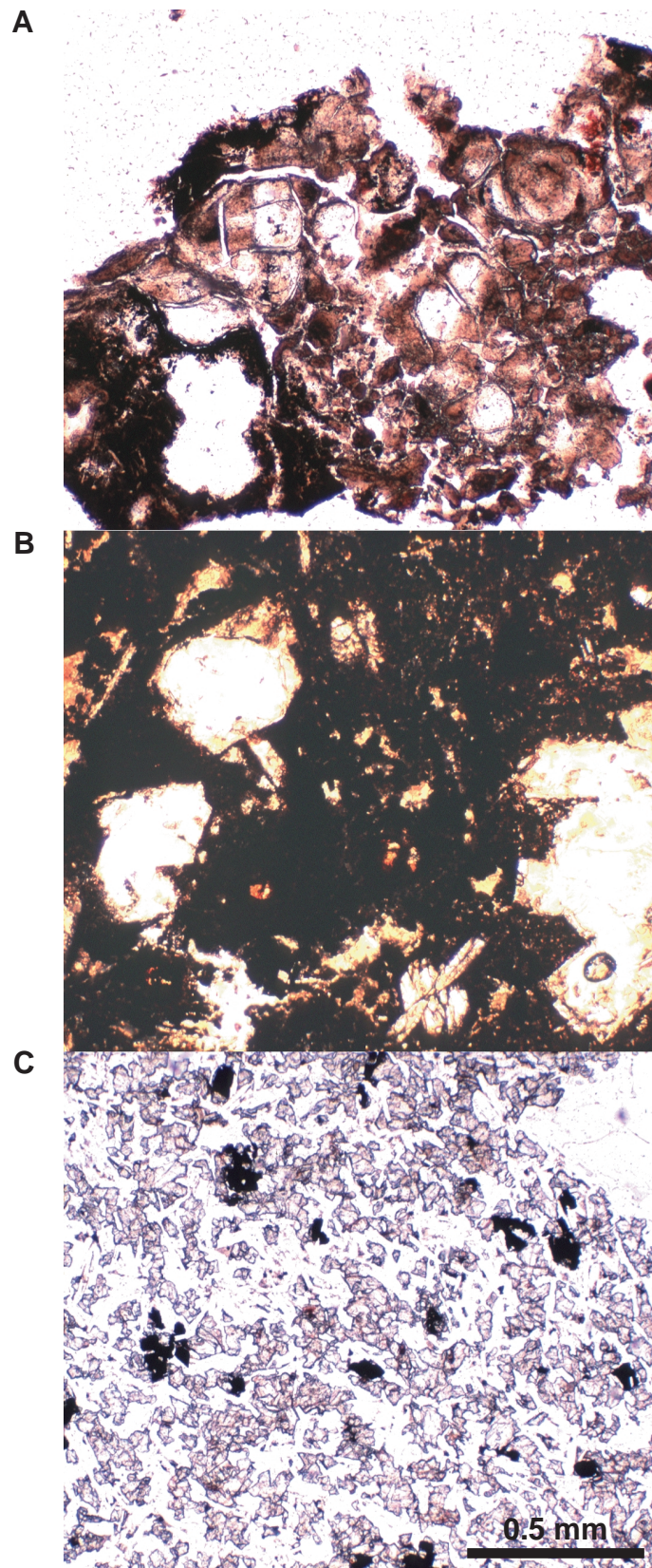


Figure 3. Representative thin section photographs of Group 1, 2, and 3 samples showing textural and mineralogical differences primarily related to various degrees of alteration. See text and Table 2 for description of the respective minicores. **A.** Interval 163-990A-12R-2, 75–77 cm. **B.** Interval 163-990A-13R-3, 31–33 cm. **C.** Interval 163-990A-9R-2, 5–7 cm.

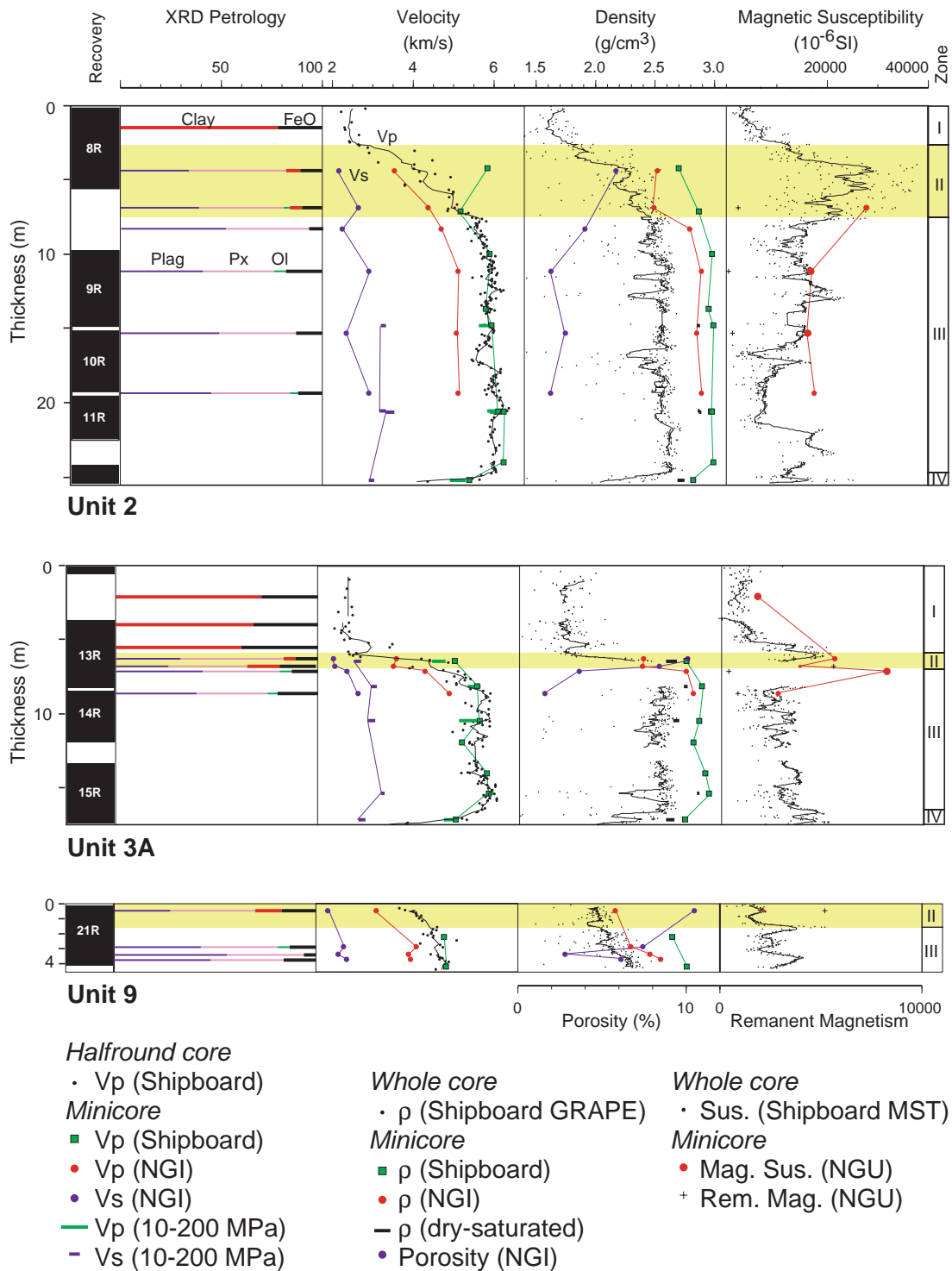


Figure 4. Petrological and physical property variations of selected basalt-flow units in Hole 990A. Sample depth values adjusted to account for missing section by linear scaling in the flow top and base. Solid black line = running-average filtered data applied as in Figure 2. See text for discussion. Sus. = susceptibility, mag. = magnetic, rem. = remanent.

sive interior, while a smaller variation of 4 to 5 km/s is observed in Unit 9 (Fig. 4). The shore-based  $P$ -wave velocities measured under atmospheric conditions show 0.5 to 1.0 km/s lower values than the shipboard data (Fig. 4; Table 2). The lithostatic pressure in the drilled basement is estimated to be 10–13 MPa, and  $P$ -wave velocities measured on 13 massive samples under 10 MPa confining pressure are

0.1 to 0.7 km/s (mean 0.4 km/s) lower than the velocities measured shipboard on the same samples (Cerney and Carlson, Chap. 3, this volume). At 200 MPa confining pressure, corresponding to ~7-km burial depth, the difference between the ship- and shore-based velocities are reduced to –0.1 to –0.2 km/s, with a mean deviation of 0.04 km/s.

The  $S$ -wave velocities are less reliable than the  $P$ -wave velocities because of the greater difficulties involved in picking the first arrivals.  $S$ -wave velocities measured under atmospheric conditions are in the range 2.0 to 2.9 km/s, with  $V_p/V_s$  values of 1.6 to 2.2 (mean 1.77).  $S$ -wave velocities measured on massive samples under 200 MPa confining pressure are in the range 2.7–3.5 km/s, with  $V_p/V_s$  values of 1.72–1.87 (Cerney and Carlson, Chap. 3, this volume).

The  $V_p$  data show that thermal and pressure relaxation and drying of the samples permanently change their elastic properties. The shipboard  $V_p$  measurements appear to be the most reliable, although microcracks may have already formed during drilling and recovery of the core. At later times the same samples have to be submitted to unrealistically high pressures (~200 MPa) to obtain results comparable with those measured immediately after the recovery.

### Density and Porosity

The shipboard GRAPE bulk density varies systematically within the flow units in a pattern similar to the  $P$ - and  $S$ -wave velocities (Fig. 4). However, there is a large scatter in the unedited GRAPE density data, and very low values are related to gaps between individual core pieces and variations in core diameter as well as to mineralogical and porosity changes. The GRAPE data were calibrated for cores within a lining. A recalibration and editing is required for hard-rock samples measured on the MST without a lining (Shipboard Scientific Party, 1996; Bückler et al., Chap. 5, this volume).

The shipboard bulk density minicore measurements are 0.3–0.4 g/cm<sup>3</sup> higher than the GRAPE bulk density data (Fig. 4). The subsequent shore-based density measurements provide intermediate values, typically 0.2–0.3 g/cm<sup>3</sup> higher than the shipboard GRAPE density values. The difference is attributed to variations in core diameter and that the GRAPE was calibrated for quartz (grain density = 2.67 g/cm<sup>3</sup>) rather than for plagioclase and pyroxene (grain density ~3.0 g/cm<sup>3</sup>).

The porosity values are generally low (2%–5%) in the massive lava interior, but increase to 10% just above the massive interval (Fig. 4). The porosity values in the vesicular Unit 9 are particularly high, decreasing downhole from 10% to 2%–6%.

### Magnetic Susceptibility

There is an overall good fit between the MST data and the minicore magnetic susceptibility values (Figs. 2, 4). The raw MST data are noisy, partly related to gaps between core pieces. The running-average smoothed susceptibility curve shows a distinctly different trend than the velocity and density data, a trend particularly well developed in Unit 2 and Subunit 3A. A susceptibility peak of ~30,000 10<sup>-6</sup> SI is found in the transition zone between the brecciated flow top and the massive interior. Low susceptibility values (<10,000 10<sup>-6</sup> SI) are recorded above the peak in the brecciated flow top, while intermediate susceptibility values of 10,000–25,000 10<sup>-6</sup> SI are found in the massive basalt interior. In addition, less well-defined peaks are sometimes apparent near the brecciated base of the flow units.

### Crossplots

Figure 5 shows the smoothed  $V_p$  plotted against selected physical and geochemical rock-sample parameters (Table 2). Data are further coded according to the petrological group and unit in which they belong. The  $V_p$ -porosity crossplot (Fig. 5B) shows an expected trend, with a clear negative correlation between porosity and velocity. Similarly, the  $V_p$ -LOI (loss on ignition, an alteration indicator) also shows an expected negative correlation (Fig. 5C).

Shales are typically highly anisotropic because of preferential alignment of clay minerals (Johnston and Christensen, 1995; Vernik and Liu, 1997). No strong preferential orientation of clay minerals is

observed in Zone I or Zone II thin sections. In fact, the clays often are pseudomorph assemblages replacing primary phenocrysts. The  $V_p/V_s$  value is generally decreasing with increasing alteration and decreasing  $V_p$  (Fig. 5A). A small decrease in the  $V_p/V_s$  value is observed for slightly altered samples from Zone III, whereas the  $V_p/V_s$  value for the same samples increases as the confining pressure is increased from 10 to 200 MPa (Cerney and Carlson, Chap. 3, this volume). Alteration will soften the rock framework and decrease the proportion of low-aspect ratio voids (Cerney and Carlson, Chap. 3, this volume). The decrease in the  $V_p/V_s$  value with increasing alteration and crack closure may be contributed to the hypothesis that the  $V_s$  is more sensitive to changes in fracture density than the  $V_p$  (Iturrino et al., 1991).

The  $V_p$ -K<sub>2</sub>O crossplot reveals a more complicated relationship. Potassium is an alteration-dependent element, and the velocity generally decreases with increasing K content for Group 2 and 3 samples (Fig. 5D). In contrast, the completely altered Group 1 samples have intermediate K values. The natural gamma-ray log mainly responds to variations in the K content in basaltic terrains (e.g., Planke, 1994), but Figure 5D shows that the natural gamma-ray log cannot be uniquely inverted to obtain the clay proportion in flood basalt provinces.

### Basalt Flow Zonation

Unit 2 and Subunit 3A may be divided into four distinct zones with different petrophysical and morphological characteristics (Fig. 4; Tables 1, 2). Zone I is the upper brecciated zone, Zone II is the upper transitional zone, Zone III is the massive interior zone, while Zone IV is the basal transitional and brecciated zone. Zones I–III further correspond in detail to the three groups identified by the petrological and geochemical analysis.

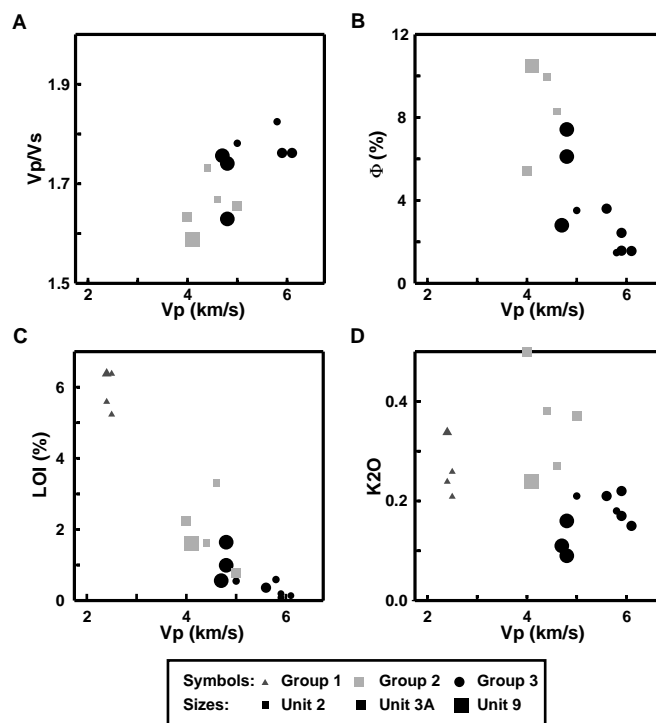


Figure 5. A.–D. Crossplots of  $V_p$  and selected physical and geochemical parameters. Symbols represent the geochemical groups (Table 2), whereas the symbol sizes represent the different flow units studied. Data from Table 2;  $V_p = V_p$  Smooth;  $V_p/V_s = \text{NGI}$  values.

*Zone I:* The upper brecciated zone is 2–7 m thick. *P*-wave velocities, densities, and magnetic susceptibilities are low and fairly constant ( $V_p = 2\text{--}3$  km/s;  $\rho = 1.6\text{--}1.8$  g/cm<sup>3</sup>; magnetic susceptibility =  $0\text{--}7.500 \cdot 10^{-6}$  SI). It is characterized by almost complete alteration to clay and iron hydroxides. The vesicularity is 0 to 20%, with fractures and veins rarely identified.

*Zone II:* The upper transitional zone is 3–5 m thick and characterized by a gradual increase of  $V_p$  from 2.5 to 5.5–6 km/s, although there is a scatter of the data (Fig. 4). Similarly, the density increases from 1.7 to 2.8 g/cm<sup>3</sup>. In contrast, the magnetic susceptibility is high, with peak values of 20,000–40,000  $10^{-6}$  SI. Alteration is intermediate, with 5%–15% modal clay and significant plagioclase alteration with modal pyroxene content greater than the plagioclase content. Porosity is relatively high, typically 5%–10%, while the vesicularity varies between 0 and 20%.

*Zone III:* The massive interior zone is 10–15 m thick. Petrophysical properties are fairly constant, with high velocities and densities and intermediate magnetic susceptibilities ( $V_p = 5.5\text{--}6$  km/s;  $\rho = 2.8\text{--}2.9$  g/cm<sup>3</sup>; magnetic susceptibility =  $5,000\text{--}20,000 \cdot 10^{-6}$  SI) and characterized by massive, largely unaltered basalt. Total porosity is generally low (<5%). Similarly, vesicularity is low (<2%), but 1-cm-thick, highly vesicular bands are identified locally. Sparsely distributed, dominantly subvertical fractures are found in this zone.

*Zones IV:* The basal transitional and brecciated zone exhibits similar properties as the combined upper transitional and brecciated zones but are only 1–2 m thick. No samples were collected for shore-based studies from this basal zone.

The four-zone structure is less well developed in the very vesicular pahoehoe basalt Unit 9. Only a 10-cm, very fragmented section was recovered from the flow top (Zone I). The thickness is poorly constrained, as 4.25 m of section is missing in Core 21R (Fig. 2). Sample 163-990A-21R-2, 30–32 cm, collected 50 cm from the flow top, has similar characteristics as the Zone II samples in Unit 2 and Subunit 3A (Table 2). Samples from deeper parts of the unit are relatively unaltered, although they show geochemical and petrological characteristics similar to the samples from Zone III in Unit 2 and Subunit 3A (Table 2; Fig. 4). The magnitude and trend of the velocity and density data differs in Unit 9. Here, the  $V_p$  increases gradually from 4.5 to 5.0 km/s, while density increases similarly from 2.4 to 2.7 g/cm<sup>3</sup>. The lower velocity and density in the interior of Unit 9, compared to Unit 2 and Subunit 3A, are clearly related to the high vesicularity of 15%–25% in the majority of this lava flow. The basal part of the flow is poorly recovered, and Zone IV is not identified.

## DISCUSSION

### Emplacement and Alteration

Recent studies suggest that continental flood basalts can be emplaced as inflated compound pahoehoe flows with a three-part internal structure of an upper crust, a lava core, and a basal zone (Hon et al., 1994; Self et al., 1996; 1997; 1998). The upper crust is highly vesicular, with hypocrySTALLINE texture (i.e., a high original glass content) and irregular jointing comprising typically 40%–50% of the total flow thickness. The lava core comprises 40%–60% of the total flow thickness. It is characterized by low vesicularity, regular jointing, and a holocrystalline texture, whereas the porosity is dominated by diktytaxitic voids between the crystals. The basal zone is thin (0.5–1 m), has a high original glass content, and has poorly developed jointing.

A three-part lava flow structure has been inferred from log and wireline data on volcanic margins (Planke, 1994), being similar to the upper crust, lava core, and basal zone internal structure seen in the

field. However, the petrophysical data from Hole 990A suggest the upper crust may actually be divided into two zones (Fig. 4) (Bücker et al., in press). This subdivision is based on the physical property measurements, but it can also be related to the severity of the post-emplacement alteration. The high initial vesicularity and jointing in the upper crust provides pathways for fluids and facilitates complete alteration of the dominantly glassy crust. Studies suggest that the initial alteration of the flow top is rapid, soon after the emplacement in a subaerial environment, and that smectite- and iron oxide-rich paleosols develop (Desprairies et al., 1989; Singer et al., 1994). During subsequent submergence of the basalt pile, the paleosols may have become relatively impermeable, and hydrothermal fluid flow may be in fractures below the highly altered layer. Such late-stage hydrothermal alteration has been proposed by Desprairies et al. (1989) and might explain the relatively high potassium content and magnetic susceptibility in the intermediately altered Zone II, compared to the highly altered Zone I and the fairly fresh Zone III (Fig. 4).

The thickness and degree of alteration appear to be related to the primary emplacement environment. The jointed, highly vesicular upper crust corresponds to the strongly and intermediately altered Zones I and II. The paleoclimate and time duration between subsequent eruptions are important parameters in determining the alteration stage and, thus, the physical properties of the lavas. The completely altered Zone I is not present in the highly vesicular Unit 9 (Fig. 4). We relate this to rapid emplacement of subsequent pahoehoe flows not providing sufficient time for a soil horizon to develop.

### Elastic Properties

Goldberg (1997) reviewed seismic wave propagation in oceanic basalts. In particular, variations in total porosity and the pore aspect ratio spectrum are commonly regarded as the major cause of velocity variations, a hypothesis substantiated by theoretical considerations and numerical modeling (e.g., Wilkens et al., 1991). In addition, oxidation and hydration alteration processes are considered to be significant in modifying the physical properties of oceanic crust with age (Johnson and Semyan, 1994).

The crack concentration and aspect ratio distribution are considered to be the main causes of velocity variations in the massive parts of subaerial lava flows. Cerney and Carlson (Chap. 3, this volume) show that the variations in measured *P*- and *S*-wave velocities in minicores from the massive parts of lavas from Hole 990A can be modeled as primarily caused by variation in total porosity. The modeling also suggests that a common pore aspect ratio distribution normalized by porosity exists within the massive parts of the upper three aa flows from Hole 990A.

The effect of clay alteration on seismic properties of flood basalts is more difficult to quantify. First, it is difficult to recover the altered zones using rotary drilling techniques. Second, very altered samples are fragile and, thus, it is difficult to measure reliable velocities in the laboratory. Third, the velocities of altered samples are often severely reduced during storage because of clay swelling.

The  $V_p$  measured under atmospheric conditions during the shore-based studies of Hole 990A is 0.5–1 km/s lower than the corresponding shipboard velocities (Table 2). We relate this difference primarily to the swelling properties of smectite as microfissures develop during storage. The dominant alteration clay mineral in Hole 990A is smectite, which is a low-temperature alteration mineral that is physically unstable because of its swelling properties (Douglas et al., 1994; McGreevy, 1982). Microfissures are developed during cyclic wetting and drying of basalts with minor amounts of smectite, leading to a deterioration of the rock, which is associated with a significant decrease in seismic velocity (McGreevy, 1982). The microfissure development is nonreversible and will also affect anisotropic measurements as the cracks develop preferentially parallel to the rock foliation (Ruiz de Argandona et al., 1995). Confining pressures have to be

increased to 200 MPa to match the original shipboard  $P$ -wave velocities (Cerney and Carlson, Chap. 3, this volume). Thus, to provide reliable data, velocity data from altered basalt cores should be measured on board ship as soon as possible after recovery or kept saturated under confining pressure.

The large mineralogical changes within Unit 2 and Subunit 3A (Fig. 4) correspond to changes in the elastic properties within the basalt units. The  $V_p$  in Zone I is very low ( $\sim 2.5$  km/s) and fairly constant. This zone is clay dominated ( $>50\%$  smectite; Fig. 4). Velocity logs in smectite-rich intervals in the North Sea show similar low velocities ( $\sim 2$  km/s) and insignificant velocity changes with depth (Thyberg et al., unpubl. data).

Numerous rock-property theories have been developed to describe changes in elastic moduli in clastic rocks consisting of clay and sand mixtures (e.g., Hansen, 1997). The three sand/clay models shown in Figure 6 cannot be used directly to predict velocity variations in altered crystalline rocks such as basalts, but they provide insight into the significance of clay minerals on the elastic properties of basalts. All three theories predict a significant decrease in velocity when the clay proportion exceeds  $\sim 30\%$ – $40\%$ . This is related to a pronounced softening of the rock when the clay minerals become a main part of the rigid rock framework. Zone II is characterized by a rapid increase in  $V_p$ . The modal clay proportion in this zone varies from 5% to 16% (Table 2). As clay minerals and iron hydroxides are part of the rigid framework, they may significantly soften the rock. But, as both the porosity and alteration mineral percentages vary in this zone, a reduction in either or both may locally contribute to the overall increase in the  $V_p$ .

### Magnetic Properties

Susceptibility and remanence values are lowest in Zone I (Fig. 4). These low magnetic values can be attributed to the hematite, a magnetic mineral with the lowest susceptibility and magnetic intensity values, which confirm the highly oxidized and altered zone (Table 2). Zone II can be subdivided into two parts characterized by the magnetic property behavior. In the upper part, the magnetic intensity is highest with moderate susceptibility values, and, in the lower part, the susceptibility is highest with lowest magnetic intensity values. This is possibly caused by two independent effects—smaller grain sizes (single domain particles) in the upper part, and larger grain sizes (multiple domain particles) in the lower part. The susceptibility behavior can be explained by a combined effect of grain size and oxidation state.

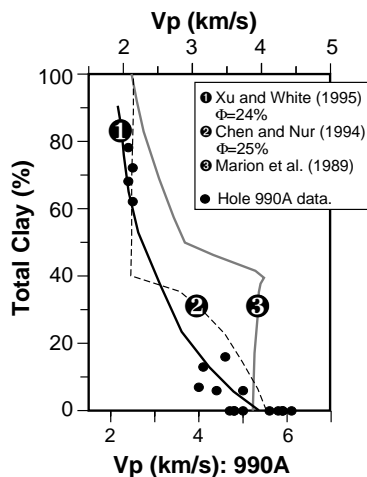


Figure 6.  $V_p$  as a function of clay content (Hansen, 1997) compared with Hole 990A clay percentage and smoothed  $V_p$  data (Table 2). Note different  $V_p$  scales. Marion et al. (1989) model assumes clay as a pore filling. Chen and Nur (1994) and Xu and White (1995) models are a critical concentration model and a modified effective medium model, respectively.

The upper part with small grain sizes could be less oxidized (maghemite), and, thus, it shows lower susceptibility values than the higher oxidized lower part (magnetite) with large grain sizes.

The fresh and unoxidized Zone III shows the original magnetic properties with low magnetic intensity values and moderate susceptibility values, pointing to magnetite with a low titanium content and relatively large grain sizes. This dense part of the flow may serve as a seal and may partly protect the lowest part of the flows against intense alteration from the top. The lower part of Zone IV again shows high magnetic intensity values and moderate susceptibility values. Because of the oxidation scheme, the magnetic mineral may be (titano)maghemite with small grain sizes.

The most prominent feature of the magnetic properties susceptibility and remanence is the high values in Zone II (Figs. 2, 4). The question is whether it is caused by primary magnetic minerals or alteration. Ore microscopy of polished thin sections suggests that the dominant magnetic mineral is magnetite with differing amounts of titanium ((titano)magnetite) (Table 2). This observation is also confirmed by studies on volcanic rocks from Leg 152 (Fukuma, 1998). (Titano)magnetite undergoes alteration during low-temperature oxidation and hydrothermal alteration. In the upper part of the lava flows, the highly vesicular and fractured texture provides pathways for fluids. In the first step of low-temperature oxidation, the (titano)magnetite is changed to (titano)maghemite (Fig. 7). This is accompanied by decreasing susceptibility and magnetization intensity and increasing Curie temperatures. In the second step, the (titano)maghemite is changed into magnetite and then further into hematite. The oxidation to magnetite is accompanied by increasing Curie temperatures, susceptibility, and magnetization intensity, whereas the oxidation to hematite lowers the susceptibility and magnetic intensity but increases the Curie temperature. It is not necessary in each case during low-temperature oxidation that the (titano)magnetite is first changed into (titano)maghemite and then into magnetite or hematite. There might also be a direct way of oxidizing (titano)magnetite into magnetite and hematite (Fig. 7). In addition to the oxidation effects on the magnetic properties, susceptibility and magnetic intensity are also dependent on the abundance of the magnetic minerals, grain-size distribution, and shape.

In summary, we suggest from the magnetic property observations that the lower parts of the highly vesicular, scoriaceous, and fractured lava top and bottom are characterized by high magnetic susceptibility and intensity caused by different states of low-temperature oxidation. During these different states of low-temperature oxidation, susceptibility and magnetic intensity may be enhanced or reduced depending on the alteration to magnetite or hematite. A secondary effect on the magnetic properties is caused by the grain-size distribution.

### Implications for Well-Log Interpretation

Wireline logs are important to link downhole core data with surface geophysical measurements and to correctly interpolate missing sections in the core data (e.g., Goldberg, 1997). Detailed core-log integration is often difficult as the accurate depth location of the cores

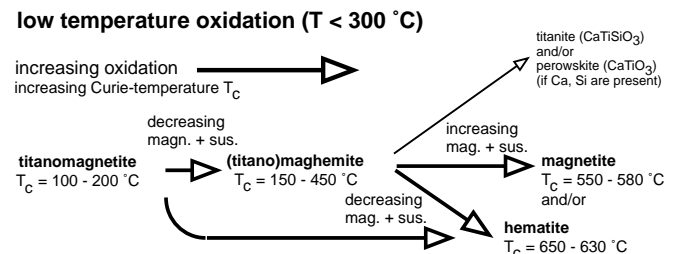


Figure 7. Behavior of the magnetic properties remanence and susceptibility, and Curie temperatures, during low temperature oxidation (modified after N. Petersen, pers. comm., 1982).

with respect to logging data frequently is impossible to obtain on the required centimeter or tens of centimeters scale. The high core recovery and densely sampled MST data and  $P$ -wave velocities from Hole 990A provide a unique data set in a flood basalt sequence. The Hole 990A core data can therefore be used to gain insight into interpretation of wireline logs recorded in flood basalt terrains. This is confirmed by downhole logging data from the nearby Hole 917A (Fig. 1) (Planke and Cambray, 1998) drilled into similar volcanic basement showing very similar intraflow variations in petrophysical logs as the Hole 990A core data. Figure 8 shows a sketch of the internal  $V_p$  variation in a thick flood basalt unit based on the Hole 990A data. The velocity data can be interpreted in terms of superimposed alteration and porosity variations and is typically represented by Unit 2 and Subunit 3A (Fig. 4).

## CONCLUSIONS

The observed large variations in petrophysical properties in Hole 990A are caused by interplay of primary lava flow emplacement structures and subsequent alteration. The initial flow emplacement generates large, primarily subhorizontal variations in textures, porosity, and permeability structure. Subsequent subaerial alteration transforms the upper flow into a clay-rich red soil layer. After burial and submergence, salt water may preferentially flow in fractures below this upper layer, providing a different alteration regime as suggested by more potassium-rich clay minerals and higher concentration of magnetic minerals. High eruption frequency will inhibit the development of a soil horizon and a less heterogeneous lava pile. The very dense lava core will remain less affected by both alteration episodes, whereas the lava base may experience an alteration development similar to the upper crust.

Modeling based on sand/clay clastic lithologies suggests a prominent softening of the rocks when the clay proportion increases above 30%–40% (i.e., when clay minerals become interlocked). In accord with this, we observe that seismic velocities within basaltic lava flows are significantly lowered when the clay proportion exceeds 50%.

Drying and wetting of only slightly altered basalts severely changes the elastic properties of the rock. This is related to microcrack development induced by the swelling properties of the alteration clay smectite.

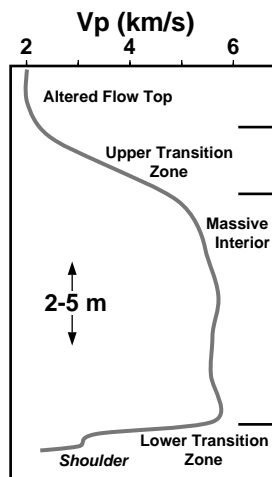


Figure 8. Schematic subaerial basalt flow zonation model based on Hole 990A core data.

## ACKNOWLEDGMENTS

We would like to sincerely thank the crew and laboratory staff on the *JOIDES Resolution* for doing a great job under very difficult circumstances. Further, invaluable help with the laboratory measurements and analysis has been provided by the Norwegian Geotechnical Institute (Gunnar Vik), the Norwegian Geological Survey (Trond Torsvik), and the University of Oslo (Berit Løken Berg, Muhammad Amir Iqbal, and Per Aagaard). Reviews from H.C. Larsen, G.I. Iturrino, R. Wilkens, and O. Eldholm were greatly appreciated. This study has been financed by the Norwegian Research Council under the PROPETRO program and by Statoil.

## REFERENCES

- Bücker, C.J., Delius, H., Wohlenberg, J., and ODP Leg 163 Shipboard Scientific Party, in press. Comparison of core and downhole measurements of ODP Legs in basaltic volcanics in the NE Atlantic. *Geol. Soc. Spec. Publ.*
- Chen, Q., and Nur, A., 1994. Critical concentration models for porous material. In Corapcioglu, M.Y. (Ed.), *Advances in Porous Media* (Vol. 2): New York (Elsevier), 169–308.
- Delius, H., Bücker, C.J., and Wohlenberg, J., 1995. Significant log responses of basaltic lava flows and volcanoclastic sediments in ODP Hole 642E. *Sci. Drill.*, 5:217–226.
- Desprairies, A., Tremblay, P., and Laloy, C., 1989. Secondary mineral assemblages in a volcanic sequence drilled during ODP Leg 104 in the Norwegian Sea. In Eldholm, O., Thiede, J., Taylor, E., et al., *Proc. ODP, Sci. Results*, 104: College Station, TX (Ocean Drilling Program), 397–409.
- Douglas, G.R., McGreevy, J.P., and Whalley, W.B., 1994. Mineralogical aspects of crack development and freeface activity in some basalt cliffs, Country Antrim, Northern Ireland. In Robinson, D.A., and Williams R.B.G. (Eds.), *Rock Weathering and Landform Evolution*: New York (Wiley & Sons), 71–88.
- Duncan, R.A., Larsen, H.C., Allan, J.F., et al., 1996. *Proc. ODP, Init. Repts.*, 163: College Station, TX (Ocean Drilling Program).
- Fukuma, K., 1998. Origin and applications of whole-core magnetic susceptibility of sediments and volcanic rocks from Leg 152. In Saunders, A.D., Larsen, H.C., and Wise, S.W., Jr. (Eds.), *Proc. ODP, Sci. Results*, 152: College Station, TX (Ocean Drilling Program), 271–280.
- Goldberg, D., 1997. The role of downhole measurements in marine geology and geophysics. *Rev. Geophys.*, 35–3.
- Hansen, O., 1997. The influence of clay minerals on acoustic properties of sandstones [Ph.D. thesis]. Norw. Univ. of Sci and Tech., Trondheim.
- Hon, K., Kauahikaua, J.P., Denlinger, R., and Mackay, K., 1994. Emplacement and inflation of pahoehoe sheet flows: observations and measurements of active lava flows on Kilauea, Hawaii. *Geol. Soc. Am. Bull.*, 106:351–370.
- Iturrino, G.J., Christensen, N.I., Becker, K., Boldreel, L.O., Harvey, P.K.H., and Pezard, P., 1995. Physical properties and elastic constants of upper crustal rocks from core-log measurements in Hole 504B. In Erzinger, J., Becker, K., Dick, H.J.B., and Stokking, L.B. (Eds.), *Proc. ODP, Sci. Results*, 137/140: College Station, TX (Ocean Drilling Program), 273–292.
- Johnson, H.P., and Semyan, S.W., 1994. Age variation in the physical properties of oceanic basalts: implications for crustal formation and evolution. *J. Geophys. Res.*, 99:3123–3134.
- Johnston, J.E., and Christensen, N.I., 1995. The seismic anisotropy of shales. *J. Geophys. Res.*, 100:5991–6003.
- Larsen, H.C., and Saunders, A.D., 1998. Tectonism and volcanism at the southeast Greenland rifted margin: a record of plume impact and later continental rupture. In Saunders, A.D., Larsen, H.C., and Wise, S.W., Jr. (Eds.), *Proc. ODP, Sci. Results*, 152: College Station, TX (Ocean Drilling Program), 503–533.
- Larsen, H.C., Saunders, A.D., Clift, P.D., et al., 1994. *Proc. ODP, Init. Repts.*, 152: College Station, TX (Ocean Drilling Program).
- Marion, D., Nur, A., and Alabert, F., 1989. Modeling the relationships between sonic velocity, porosity, permeability and shaliness in sand shale and shaley sand. *SPWLA 13th Annu. Logging Symp.*, 1–22.
- McGreevy, J.P., 1982. Hydrothermal alteration and earth surface rock weathering: a basalt example. *Earth Surf. Processes Landforms*, 7:189–195.
- Petschick, R., 1997. MacDiff 3.2.6 Manual. <http://servermac.geologi.uni-frankfurt.de/Rainer.html>. Johann Wolfgang Goethe-Univ. Frankfurt am Main, Germany.

- Planke, S., 1994. Geophysical response of flood basalts from analysis of wireline logs: Ocean Drilling Program Site 642, Vøring volcanic margin. *J. Geophys. Res.*, 99:9279–9296.
- Planke, S., and Cambray, H., 1998. Seismic properties of flood basalts from Hole 917A downhole data, southeast Greenland volcanic margin. In Saunders, A.D., Larsen, H.C., and Wise, S.W., Jr. (Eds.), *Proc. ODP, Sci. Results*, 152: College Station, TX (Ocean Drilling Program), 453–462.
- Planke, S., and Eldholm, O., 1994. Seismic response and construction of seaward dipping wedges of flood basalts: Vøring volcanic margin. *J. Geophys. Res.*, 99:9263–9278.
- Ruiz de Argandoña, V.G. Calleja, L., and Suárez del Río, L.M., 1995. Acoustic emission during swelling and contraction tests. *Eng. Geol.*, 39:147–150.
- Self, S., Keszthelyi, L., and Thordarson, T., 1998. The importance of pahoehoe. *Annu. Rev. Earth Planet. Sci.*, 26:81–110.
- Self, S., Thordarson, T., and Keszthelyi, L., 1997. Emplacement of continental flood basalt lava flows. In Mahoney, J.J., and Coffin, M. (Eds.), *Large Igneous Provinces: Continental, Oceanic, and Planetary Flood Volcanism*. Am. Geophys. Union., Geophys. Monogr., 100:381–410.
- Self, S., Thordarson, T., Keszthelyi, L., Walker, G.P.L., Hon, K., Murphy, M.T., Long, P., and Finnemore, S., 1996. A new model for the emplacement of Columbia River Basalts as large, inflated pahoehoe lava flow fields. *Geophys. Res. Lett.*, 23:2689–2692.
- Shipboard Scientific Party, 1996. Site 990. In Duncan, R.A., Larsen, H.C., Allan, J.F., et al., *Proc. ODP, Init. Repts.*, 163: College Station, TX (Ocean Drilling Program), 47–68.
- Singer, A., Wieder, M., and Gvirtzman, G., 1994. Paleoclimate deduced from some early Jurassic basalt-derived paleosols from northern Israel. *Palaeogeogr., Palaeoclimatol., Palaeoecol.*, 111:73–82.
- Symonds, P.A., Planke, S., Frey, Ø., and Skogseid, J., 1998. Volcanic eruption of the Western Australian continental margin and its implications for basin development. *West. Austral. Basin Symp.*
- Vernik, L., and Liu, X., 1997. Velocity anisotropy in shales: a petrophysical study. *Geophysics*, 62:521–532.
- Wilkens, R.H., Fryer, G.J., and Karsten, J., 1991. Evolution of porosity and seismic structure of upper oceanic crust: importance of aspect ratios. *J. Geophys. Res.*, 96:17891–17995.
- Xu, S., and White, R.E., 1995. A new velocity model for clay-sand mixtures. *Geophys. Prospect.*, 43:91–118.

**Date of initial receipt: 12 January 1998**

**Date of acceptance: 13 November 1998**

**Ms 163SR-105**